Dynamics of the phospholipid shell of microbubbles: a fluorescence photoselection and spectral phasor approach

DOI: 10.1039/c8cc01012a
Handle: http://hdl.handle.net/1942/26058

ChemComm

Accepted Manuscript

This article can be cited before page numbers have been issued, to do this please use: E. Slenders, S. Seneca, S. K. Pramanik, N. Smisdom, P. Adriaensens, M. vandeVen, A. Ethirajan and M. Ameloot, *Chem. Commun.*, 2018, DOI: 10.1039/C8CC01012A.

This is an Accepted Manuscript, which has been through the Royal Society of Chemistry peer review process and has been accepted for publication.

Accepted Manuscripts are published online shortly after acceptance, before technical editing, formatting and proof reading. Using this free service, authors can make their results available to the community, in citable form, before we publish the edited article. We will replace this Accepted Manuscript with the edited and formatted Advance Article as soon as it is available.

You can find more information about Accepted Manuscripts in the author guidelines.

Please note that technical editing may introduce minor changes to the text and/or graphics, which may alter content. The journal's standard Terms & Conditions and the ethical guidelines, outlined in our author and reviewer resource centre, still apply. In no event shall the Royal Society of Chemistry be held responsible for any errors or omissions in this Accepted Manuscript or any consequences arising from the use of any information it contains.

ROYAL SOCIETY OF CHEMISTRY

rsc.li/chemcomm

View Article Online
DOI: 10.1039/C8CC01012A

Journal Name

ARTICLE TYPE

Cite this: DOI: 10.1039/xxxxxxxxxx

Dynamics of the phospholipid shell of microbubbles: a fluorescence photoselection and spectral phasor approach†

Eli Slenders,[a] Senne Seneca,[bc] Sumit Kumar Pramanik,[bcd] Nick Smisdom,[a] Peter Adriaensens,[bc] Martin vandeVen,[a] Anitha Ethirajan,[bc‡] and Marcel Ameloot[a‡]

Received Date
Accepted Date

DOI: 10.1039/xxxxxxxxxx

www.rsc.org/journalname

The lipid organization of microbubbles is important in many applications. By monitoring the photoselection and emission spectrum of the fluorescent probe Laurdan in perfluorobutane gas–filled DPPC microbubbles with a two–photon laser scanning microscope, we observed a transition to a more rigid lipid organization in 30 minutes to several hours.

Microbubbles are particles between 0.1 and 100 μm in diameter comprising a gas core that is encapsulated by a stabilizing surfactant shell.[1] These spherical structures find numerous applications, including gas delivery, controlled release of a therapeutic payload for targeted therapy, contrast enhancement in ultrasound imaging, personal care products, aerated food, and foamed construction materials.[2–10] Containers with a lipid monolayer shell are also used as a bioprinting tool for the fabrication of living tissues through scaffold cell seeding.[11] In all these applications, knowledge of the organization and stability of the monolayer shell is crucial. These properties are highly influenced by the composition of the particle. Previously, lipids, lipid mixtures, polymer surfactants and proteins, or combinations of these ingredients, have been used to design improved stability against rupture, enhanced circulation time in the body, stability against gas dissolution, and target specificity.[12–15] The choice of lipid or lipid mixture, but also of the encapsulated gas, influences the temperature–dependent organization of these lipids[16] and allows to tune the rigidity of the shell.[17]

A fast and sensitive method is needed to characterize the shell structure of individual microbubbles, *i.e.* to obtain information on the shell rigidity and the lipid organization. Here, we describe a non–invasive optical method based on linearly polarized two–photon illumination of Laurdan stained microbubbles.

The fluorescence intensity of Laurdan can be linked to the orientation of the chromophore with respect to the polarization orientation of the incident light, see Supporting Information (SI) paragraph *Laurdan fluorescence* and Fig. S1. The brightest emission signal is obtained when the absorption transition dipole of the chromophore is aligned parallel to the polarization direction of the excitation light. For increasing angles θ between the chromophore dipole and the polarization direction, the fluorescence intensity will decrease and ultimately vanish for $\theta = 90\ ^\circ$. This photoselection effect follows a $\cos^2\theta$ relationship for one–photon excitation and a more pronounced $\cos^4\theta$ angular dependence for two–photon excitation (2PE).[18,19]

In addition, the Laurdan fluorescence emission spectrum depends on the polarity of its immediate environment.[20,21] In case of phospholipid vesicles in water, the Laurdan emission spectrum maximum exhibits a large red Stokes' shift of 50 *nm* – from 440 *nm* to 490 *nm* – when going from the gel to the liquid crystalline lipid phase. This pronounced spectral shift originates from a higher degree of dipolar relaxation of water molecules above the phase transition compared to the gel phase, since more water molecules are surrounding the Laurdan probe in the former situation.[22,23] Consequently, the fluorescence emission spectrum of Laurdan provides information on the local organization of the lipids, as demonstrated in bilayers by a plethora of researchers.[19–22,24–33]

Spectral changes can be conveniently quantified with the gen-

[a] *Biomedical Research Institute (BIOMED), Hasselt University, Agoralaan Bldg. C, 3590 Diepenbeek, Belgium. Fax: +32 (0) 1126 9299; Tel: +32 (0) 1126 9233; E-mail: marcel.ameloot@uhasselt.be; anitha.ethirajan@uhasselt.be*

[b] *Institute for Materials Research (IMO), Hasselt University, Wetenschapspark 1 and Agoralaan Bldg. D, 3590 Diepenbeek, Belgium.*

[c] *IMEC, associated lab IMOMEC, Wetenschapspark 1, 3590 Diepenbeek, Belgium.*

[d] *Current affiliation: CSIR–Central Salt & Marine Chemicals Research Institute, Bhavnagar 364002, Gujarat, India*

† Electronic Supplementary Information (ESI) available, containing details on the microbubble preparation, the chemical characterization, the fluorescence spectra, microscopy imaging and the generalized polarization analysis. See DOI: 10.1039/b000000x/

‡ These authors contributed equally to this work.

View Article Online
DOI: 10.1039/C8CC01012A

eralized polarization (GP) approach. For an idealized instrument, the GP is defined as[20]

$$GP = \frac{I_B - I_R}{I_B + I_R}, \quad (1)$$

with I_B and I_R the Laurdan fluorescence intensity in the blue (440 nm) and green (490 nm) channel, respectively. GP values range from $+1$ when the Laurdan molecules are mainly emitting in the blue wavelength range to -1 for a red–shifted spectrum with the Laurdan located in a highly polar environment. For GP imaging, the microscopy setup must be calibrated at sample temperature with a reference spectrum, as shown in the SI, Figs. S3 and S4.

Here, we combine imaging of the GP of Laurdan stained microbubbles with fluorescence intensity measurements at different orientations of the linear excitation polarization. We apply this approach to study the lipid shell structure of 1,2–dipalmitoyl–*sn*–glycero–3–phosphocholine (DPPC) microbubbles, filled with the non–toxic, inert perfluorobutane (PFB) gas. Using DPPC, Zuo[34] showed that the monolayer and bilayer phase behavior was similar. We measure the local effective lateral layer rigidity based on 2PE fluorescence imaging with two–channel GP detection and determine the Laurdan chromophore orientation with respect to the shell surface. Dynamic changes in the microbubble shell structure are recorded in time series spanning several hours. Experiments are conducted at room temperature and close to the phase transition temperature of DPPC in vesicles (41.4 $^\circ C$[35]), to mimic physiological pyrexia conditions. Details on the microbubble preparation using a two–step sonication protocol, the fluorescence spectra of shell sections of individual bubbles, cross–sections, the imaging conditions and the GP analysis protocol are described in the SI.

Fig. 1 and section 3 of the SI provide an overview of the microbubble imaging and GP analysis results. The majority of the microbubbles exhibit an intensity distribution similar to the first row of Fig. 1, *i.e.* with the top (T) and bottom (B) part brighter than the left (L) and right (R) side. Since the illumination light is horizontally polarized, these images indicate that the absorption dipole of the chromophoric moiety of Laurdan is, surprisingly, mainly aligned with the microbubble shell surface. This result is in stark contrast to earlier observations of Laurdan stained lipid bilayers made by others on giant unilamellar vesicles[25,26,28] where the polarization dependence of the fluorescence of Laurdan is rotated over 90 ° with respect to our observations and has maximal intensity at the L and R sides. Rotating the polarization direction of the incident laser light confirms the orientation of the absorption dipole with respect to the shell surface, see Fig. S5.

In some Laurdan stained microbubbles, however, the photoselection effect creates a brighter L and R side compared to the T and B side, as illustrated in the second row of Fig. 1. In these cases, the chromophore dipoles are apparently oriented perpendicularly to the shell surface, pointing radially. We observed this behavior both at 25 $^\circ C$ and at 42 $^\circ C$, see Fig. S6.

Microbubbles with a clear T–B photoselection pattern systematically have a lower average GP than bubbles with a clear L–R pattern, as shown in the last column of Fig. 1. In the T–B case,

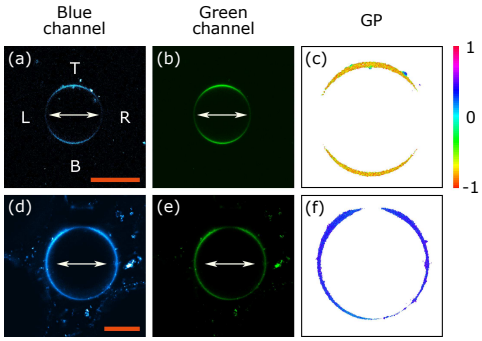

Fig. 1 Photoselection and Generalized Polarization (GP) observed in Laurdan stained DPPC–PFB microbubbles imaged with 2PE laser scanning microscopy at 25 $^\circ C$. Column 1 (a, d): blue Laurdan fluorescence emission channel (BP 405-455 nm). Column 2 (b, e): green Laurdan fluorescence emission channel (BP 475-565 nm). Right column (c, f): GP calculated pixel wise from the blue and green images. Top row images show bright top (T) and bottom (B) shell regions, while the left (L) and right (R) side emit less fluorescence. The Laurdan molecules below and above the focal plane will contribute more to the observed signal in the T–B part than in the L–R part, *i.e.* the apparent slice thickness varies with the intensity, creating the illusion of thicker T–B shell segments compared to the L and R sides, top row. The second row images exhibit an opposite pattern. GP values are indicated by the upper right color bar. The excitation polarization is horizontal, as illustrated with the white arrows. Illumination wavelength is 780 nm. Scale bars are 50 μm and hold for the first two columns. The microbubbles in the GP panels are set to the same diameter. Brightness and contrast are individually adjusted for all images for visualization purposes. The full overview, including similar results at 42 $^\circ C$, is shown in Fig. S6.

the GP values are highly negative. In contrast, in the L–R case, these are closer to zero or positive.

Clearly, the L–R fluorescence intensity pattern and the high GP values in the second row in Fig. 1 demonstrate that the lipid shell structure of some microbubbles can differ significantly from other microbubbles within the ensemble. Moreover, a microbubble containing simultaneously both the low and the high GP phase was found, as shown in Fig. S11. To determine whether a microbubble shell may evolve from one state to the other, we imaged individual microbubbles in a time series spanning several hours. For each pair of blue and green channel images, the GP values were computed pixel wise and plotted in a histogram. We evaluated each histogram with the first–order phasor calculation.[36,37] This model–free method converts each histogram into a single point (G, S) within the unit circle, allowing a convenient representation of the temporal evolution of the GP, see Fig. S7 in the SI for the analysis of a representative microbubble, and also the detailed protocol. The resulting phasor plot is shown in Fig. 2. A video of the lipid dynamics during the transition is presented in *Fig_S9_time_series.mp4*.

At the start of the time lapse measurement, the microbubble has a T–B photoselection effect and a negative GP, similarly to the first row of Fig. 1. The corresponding histogram leads to a data point in the lower left quadrant of the phasor plot. During the first 90 minutes, consecutive images all yield similar (G, S) locations. Then, the microbubble starts shrinking, as shown in panel (a) of Fig. S10. The angular intensity distribution rotates 90 ° and the blue channel fluorescence becomes brighter than the green chan-

View Article Online
DOI: 10.1039/C8CC01012A

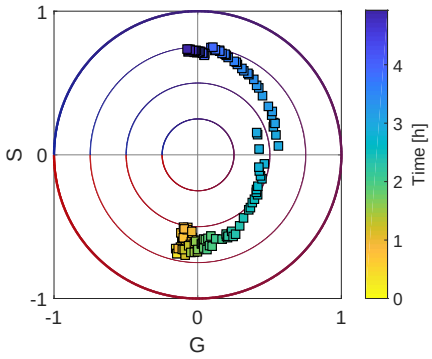

Fig. 2 Phasor plot of the shell dynamics at 25 °C of a single Laurdan stained DPPC–PFB gas–filled microbubble collected over a time interval of almost five hours. From each pair of blue and green channel fluorescence images, a histogram of GP values is calculated and analyzed with the phasor method, resulting in a pair of (G, S) coordinates for each time point. Data points are colored according to the progress in time using the color bar at the right.

nel signal. In the phasor plot, the data points move progressively counterclockwise ending up in the upper left quadrant almost 3 hours after the start of the shrinking process. During the last 40 minutes of the measurement, the bubble is in a stable configuration, with no significant change in radius or phasor coordinates.

Additional representative cases are plotted in Fig. S8 (SI). The phasor calculation of 21 individual microbubbles at a single time point shows two main classes of shell rigidity with different fluorescence intensity patterns and one microbubble undergoing the transition towards the more rigid shell class.

The observed T–B selection and the corresponding GP images can be explained by several models. Unlike for most lipid bilayers, where the dipole moments of the Laurdan chromophores are mainly oriented perpendicularly to the membrane surface, aligned with the lipid chains, the Laurdan chromophore moiety in microbubbles is preferentially oriented parallel to the shell surface. A similar result was obtained by Bagatolli *et al.* on giant liposomes composed of the polar lipid fraction E from the thermoacidophilic archaebacterial Sulfolobus acidocaldarius.[38] Bagatolli *et al.* concluded that the most plausible configuration for the observed Laurdan photoselection effect in the archaebacteria is that the chromophoric naphthalene ring is located in the lipid polar headgroup region with the absorption dipole essentially aligned parallel to the membrane surface, while the lauroyl tail is parallel to the lipid hydrocarbon chain, pointing radially. In this way, the polar carbonyl group is close to the water environment and the apolar acyl chain is surrounded by the hydrophobic lipid tails. The possibility for this L–shape conformation of Laurdan has been theoretically confirmed in DPPC vesicles in the liquid crystalline state[29] and for DOPC lipid bilayers.[39] Furthermore, the low GP values indicate a strong dipolar relaxation effect, confirming the close proximity of water molecules surrounding the Laurdan chromophore.[20]

Alternatively, the lipid tails may be oriented nearly parallel to the shell surface instead of pointing towards the center of the microbubbles. This configuration seems feasible, since the PFB gas is lipophobic[40] and the lipid density in the shell may not be high enough to force the lipid tails to point radially inwards. In this situation, the Laurdan molecules will adopt an elongated configuration and will be aligned with the shell surface with the carbonyl group pointing towards the water environment. As a result, a T–B photoselection effect combined with a negative GP can be expected. A similar surmised tail model was found by the group of Roke for sodium dodecyl sulfate at the oil–in–water droplet liquid/liquid interface.[41]

The temporal evolution of the microbubble can be explained in the context of PFB gas diffusion. Dependent on the diameter, the initial PFB gas content and the density of the lipid shell surrounding the gas bubble, the PFB gas may diffuse at different rates from the microbubble core to the medium environment. A deflating microbubble will shrink and the increasing lipid density may change the lipid organization in the shell. The observed Laurdan photoselection effects and the GP values indicate that after the shrinking process, less water molecules are surrounding the chromophores, which are then oriented perpendicularly to the shell surface. We present a possible model to explain this behavior.

Upon shrinking of the microbubble, the lipid to gas ratio increases. Assuming not all of the excess lipids will be shed from the bubble shell in the form of vesicles or lipid aggregates, the lipid concentration per unit area will rise and will force the molecules to reorganize from a loosely covered shell to a more densely packed configuration.[42] The lipid heads will move closer to each other, pushing the hydrophobic tails into the gas core. Consequently, the Laurdan molecules will also move inwards and will adopt the elongated conformer configuration,[29] due to the increased density of the lipid tails. The naphthalene groups can populate the phospholipid glycerol region,[43] with the long naphthalene axis parallel to the shell normal. The carbonyl groups will reside below the hydrophobic–hydrophilic interface.[29] GP values will turn positive when the number of water molecules surrounding the Laurdan naphthalene groups decreases. A changing orientation of the chromophore moiety results in an L–R photoselection intensity pattern upon horizontally polarized illumination. Fig. S11 (SI) indicates that this process may start locally in a small segment of the bubble. Alternatively, the whole shell structure may simultaneously, but gradually, undergo the transition, as observed in the time series measurement presented in Fig. S9 (SI). Fig. S2 provides an overview of the proposed models.

Our model for the Laurdan position and orientation in the shrunken microbubble is comparable to the expected behavior of Laurdan in a lipid bilayer in the gel phase.[29] Furthermore, the positive GP values found in DPPC vesicles below the phase transition temperature[22,28] are close to our observations of the shrunken microbubbles, both at room temperature and at 42 °C. However, it cannot be concluded that the lipid structure in a gas–filled, shrunken microbubble is similar to the organization of a bilayer. Photoselection and GP measurements on Laurdan stained giant unilamellar vesicles showed a temperature driven change in GP values upon going through the phospholipid main phase transition, while the angular distribution of the fluorescence intensity did not change.[44] In contrast, we did not observe a temperature dependence of neither the GP values nor the photoselection ef-

View Article Online
DOI: 10.1039/C8CC01012A

fect. Instead, we measured a transition in which the shell rigidity increases and the angular intensity distribution switches from T–B to to L–R. The simultaneous shrinkage of the microbubble suggests that this transition can be induced by diffusion of the PFB gas and increased lipid density. Investigating the Laurdan behavior as a function of the environmental pressure could provide a more detailed answer on the shell behavior during the transition. Our observations would also benefit from detailed calculations of the interactions between PFB gas and lipids – as lipid tail cooperativity may be influenced by PFB gas[45–47] – which is outside the scope of the present communication.

In conclusion, the lipid organization of the lipid shell of microbubbles was investigated by a microfluorimetric approach using the lipid probe Laurdan which is sensitive to water molecule proximity. By changing the excitation polarization direction, we have shown that the Laurdan chromophore is surprisingly oriented mainly parallel to the shell surface in gas–filled DPPC–PFB microbubbles. The negative GP values indicate a low shell rigidity, implying a high penetration of water molecules. However, some microbubbles revealed a 90 ° rotated intensity pattern, combined with higher GP values, indicating a restricted penetration of water molecules. We observed this effect both at 25 $^{\circ}C$ and at 42 $^{\circ}C$. We demonstrated with a time series measurement that this complex behavior relates to shrinking of the microbubbles, induced by PFB gas diffusing into the surrounding air saturated medium.

This fast and sensitive linearly polarized illumination approach as described will aid selection and sorting of lipid shell encapsulated gas–filled microbubbles. The non–invasive optical methods presented here provide a useful extension to the Spectral Imaging Toolbox provided by Aron *et al.*[48] for the characterization of individual microbubbles. This extension opens the path for screening and sorting through the use of phasor plots of individual microbubble shells and sections thereof, or through a photoselection analysis. This may contribute to designing microbubbles with a shell rigidity optimized for specific (bio–)engineering applications.

The authors thank IOF funding of Hasselt University and the support from Interuniversity Attraction Poles Program (IAP FS2 P7/05, Functional Supramolecular Systems) initiated by the Belgian Science Policy Office). The authors thank the province of Limburg for the support through IMPTECHNO. S.S. is an SB PhD fellow at the Research Foundation Flanders (FWO). The authors are grateful to Dr. R. Paesen for the development of the polarization control unit in the confocal laser scanning microscope. The authors thank H. Penxten for the technical assistance with the fluorescence spectroscopy measurements.

Conflict of interest

There are no conflicts to declare.

References

1 M. Borden, *Soft Matter*, 2009, **5**, 716–720.
2 F. Forsberg, D. A. Merton, J. B. Liu, L. Needleman and B. B. Goldberg, *Ultrasonics*, 1998, **36**, 695–701.
3 S. B. Feinstein, *Am. J. Physiol.-Heart C.*, 2004, **287**, H450–H457.
4 J. R. Lindner, *Nat. Rev. Drug Discov.*, 2004, **3**, 527–532.
5 K. Ferrara, R. Pollard and M. Borden, *Annu. Rev. Biomed. Eng.*, 2007, **9**, 415–447.
6 E. Dressaire, R. Bee, D. C. Bell, A. Lips and H. A. Stone, *Science*, 2008, **320**, 1198–1201.
7 N. Nomikou, C. Fowley, N. M. Byrne, B. McCaughan, A. P. McHale and J. F. Callan, *Chem. Commun.*, 2012, **48**, 8332–8334.
8 D. D. Cokkinos, E. Antypa, I. Kalogeropoulos, D. Tomais, E. Ismailos, I. Matsiras, S. Benakis and P. N. Piperopoulos, *Insights Imaging*, 2013, **4**, 185–98.
9 S. M. Fix, M. A. Borden and P. A. Dayton, *J. Control. Release*, 2015, **209**, 139–149.
10 T. O'Shea, J. Bamber, D. Fontanarosa, S. van der Meer, F. Verhaegen and E. Harris, *Phys. Med. Biol.*, 2016, **61**, R90–R137.
11 A. D. Graham, S. N. Olof, M. J. Burke, J. P. K. Armstrong, E. A. Mikhailova, J. G. Nicholson, S. J. Box, F. G. Szele, A. W. Perriman and H. Bayley, *Sci. Rep. UK*, 2017, **7**, 11.
12 M. M. Lozano and M. L. Longo, *Langmuir*, 2009, **25**, 3705–12.
13 T. Segers, L. de Rond, N. de Jong, M. Borden and M. Versluis, *Langmuir*, 2016, **32**, 3937–44.
14 S. Sirsi and M. Borden, *Bubble Sci. Eng. Technol.*, 2009, **1**, 3–17.
15 S. R. Sirsi and M. A. Borden, *Adv. Drug Deliver. Rev.*, 2014, **72**, 3–14.
16 B. Venegas, M. R. Wolfson, P. H. Cooke and P. L. G. Chong, *Biophys. J.*, 2008, **95**, 4737–4747.
17 I. Lentacker, S. C. De Smedt and N. N. Sanders, *Soft Matter*, 2009, **5**, 2161–2170.
18 L. A. Bagatolli, *BBA-Biomembranes*, 2006, **1758**, 1541–1556.
19 U. Bernchou, J. Brewer, H. S. Midtiby, J. H. Ipsen, L. A. Bagatolli and A. C. Simonsen, *J. Am. Chem. Soc.*, 2009, **131**, 14130–14131.
20 T. Parasassi, G. De Stasio, G. Ravagnan, R. M. Rusch and E. Gratton, *Biophys. J.*, 1991, **60**, 179–189.
21 T. Parasassi and E. Gratton, *J. Fluoresc.*, 1995, **5**, 59–69.
22 T. Parasassi, E. Gratton, W. M. Yu, P. Wilson and M. Levi, *Biophys. J.*, 1997, **72**, 2413–2429.
23 L. A. Bagatolli, in *Laurdan Fluorescence Properties in Membranes: A Journey from the Fluorometer to the Microscope*, ed. Y. Mely and G. Duportail, Springer-Verlag Berlin Heidelberg, 2012, pp. 3–35.
24 T. Parasassi, G. De Stasio, A. Dubaldo and E. Gratton, *Biophys. J.*, 1990, **57**, 1179–1186.
25 L. A. Bagatolli and E. Gratton, *Biophys. J.*, 1999, **77**, 2090–2101.
26 L. A. Bagatolli and E. Gratton, *Biophys. J.*, 2000, **78**, 290–305.
27 K. Gaus, E. Gratton, E. P. W. Kable, A. S. Jones, I. Gelissen, L. Kritharides and W. Jessup, *P. Natl. Acad. Sci. USA*, 2003, **100**, 15554–15559.
28 S. A. Sanchez, M. Tricerri, G. Gunther and E. Gratton, *Modern Research and Educational Topics in Microscopy*, 2007, 1007–1014.
29 G. Parisio, A. Marini, A. Biancardi, A. Ferrarini and B. Mennucci, *J. Phys. Chem. B*, 2011, **115**, 9980–9989.
30 O. Golfetto, E. Hinde and E. Gratton, *Methods Mol. Biol.*, 2015, **1232**, 273–90.
31 W. Kulig, A. Olzynska, P. Jurkiewicz, A. M. Kantola, S. Komulainen, M. Manna, M. Pourmousa, M. Vazdar, L. Cwiklik, T. Rog, G. Khelashvili, D. Harries, V. V. Telkki, M. Hof, I. Vattulainen and P. Jungwirth, *Free Radical Bio. Med.*, 2015, **84**, 30–41.
32 W. Kulig, P. Jurkiewicz, A. Olzynska, J. Tynkkynen, M. Javanainen, M. Manna, T. Rog, M. Hof, I. Vattulainen and P. Jungwirth, *BBA-Biomembranes*, 2015, **1848**, 422–432.
33 M. Amaro, F. Reina, M. Hof, C. Eggeling and E. Sezgin, *J. Phys. D Appl. Phys.*, 2017, **50**, 9.
34 Y. Y. Zuo, R. M. Chen, X. J. Wang, J. L. Yang, Z. Policova and A. W. Neumann, *Langmuir*, 2016, **32**, 8501–8506.
35 P. Losada-Perez, N. Mertens, B. de Medio-Vasconcelos, E. Slenders, J. Leys, M. Peeters, B. van Grinsven, J. Gruber, C. Glorieux, H. Pfeiffer, P. Wagner and J. Thoen, *Adv. Cond. Matter Phys.*, 2015, 1–14.
36 F. Fereidouni, A. N. Bader and H. C. Gerritsen, *Opt. Express*, 2012, **20**, 12729–12741.
37 L. Malacrida, E. Gratton and D. M. Jameson, *Methods Appl. Fluores.*, 2015, **3**, 047001.
38 L. Bagatolli, E. Gratton, T. K. Khan and P. L. G. Chong, *Biophys. J.*, 2000, **79**, 416–425.
39 S. Osella, N. A. Murugan, N. K. Jena and S. Knippenberg, *J. Chem. Theory Comput.*, 2016, **12**, 6169–6181.
40 J. G. Riess, *Chemical Reviews*, 2001, **101**, 2797–2919.
41 H. B. de Aguiar, M. L. Strader, A. G. F. de Beer and S. Roke, *J. Phys. Chem. B*, 2011, **115**, 2970–2978.
42 V. Knecht, M. Muller, M. Bonn, S. J. Marrink and A. E. Mark, *J. Chem. Phys.*, 2005, **122**, 024704.
43 T. Parasassi, E. K. Krasnowska, L. Bagatolli and E. Gratton, *J. Fluoresc.*, 1998, **8**, 365–373.
44 L. A. Bagatolli, S. A. Sanchez, T. Hazlett and E. Gratton, *Biophotonics, Pt A*, 2003, **360**, 481–500.
45 F. Gerber, M. P. Krafft, T. F. Vandamme, M. Goldmann and P. Fontaine, *Biophys. J.*, 2006, **90**, 3184–92.
46 M. P. Krafft and J. G. Riess, *J. Polym. Sci. A1*, 2007, **45**, 1185–1198.
47 M. P. Krafft, *J. Fluorine Chem.*, 2015, **177**, 19–28.
48 M. Aron, R. Browning, D. Carugo, E. Sezgin, J. B. de la Serna, C. Eggeling and E. Stride, *BMC Bioinformatics*, 2017, **18**, 8.

View Article Online
DOI: 10.1039/C8CC01012A